Neurochemical Research (2019) 44:2092–2102
https://doi.org/10.1007/s11064-019-02846-w

ORIGINAL PAPER

Diagnostic Efficacy of ^{18}F-FDG PET/MRI in Peripheral Nerve Injury Models

Jung Woo Nam[1,2] · Mi Jee Lee[1] · Hyung Jun Kim[1]

Received: 20 March 2019 / Revised: 14 July 2019 / Accepted: 24 July 2019 / Published online: 3 August 2019

Abstract

The aim of this study was to evaluate the diagnostic efficacy of ^{18}F-FDG PET/MRI in two different peripheral neuropathic pain models using the injured rat sciatic nerves. Twelve rats, with operation on left sciatic nerves, were evenly divided into three groups: sham surgery (control group), crushing injury and chronic constriction injury (CCI) (experimental groups). The nerve damage was assessed at 3 weeks postoperatively using following methods: paw withdrawal threshold values (RevWT), maximum standardized uptake values on PET/MRI images (*SUVR*), and counting the number of myelinated axons in proximal and distal sites of nerve injury (MAxR). The results were quantified and statistically analyzed. Compared to the control group, the crushing injury demonstrated significant differences in RevWT ($p < 0.0001$) and *SUVR* ($p = 0.027$) and the CCI group demonstrated significant differences in RevWT ($p < 0.0001$), *SUVR* ($p = 0.001$) and MAxR ($p = 0.048$). There were no significant differences between the two experimental groups for all assessments. Correlation analysis demonstrated that RevWT and *SUVR* assessments were highly correlated (r = -− 0.710, $p = 0.010$), and *SUVR* and MAxR were highly correlated (r = 0.611, $p = 0.035$). However, there was no significant correlation between RevWT and MAxR. The PET scan may be a valuable imaging modality to enable noninvasive, objective diagnosis of neuropathic pain caused by peripheral nerve injury. Also, MRI fused with PET may help clarify the anatomic location of soft tissue structures, including the peripheral nerves.

Keywords Peripheral nerve injury · Chronic constriction injury (CCI) · Crushing injury · ^{18}F-fluorodeoxyglucose (^{18}F-FDG) · Positron emission tomography (PET) · Magnetic resonance imaging (MRI)

Introduction

Peripheral nerve damage caused by nerve injuries such as trauma, compression, hypoxia, inflammation, over-stimulation, and chemical damage can result in chronic neuropathic pain, characterized by sensory abnormalities such as dysesthesia, hyperalgesia, and allodynia [1]. Such injuries can induce fiber degeneration and alterations in channel expression and composition, which lead to ectopic firing and faulty signal transmission of nerves. Satellite glial cells and autonomic neurons can incur pain-promoting states though alterations in their overall quantity, distribution, sprouting pattern, and channel expression [1]. Recently, the prevalence of dental patients suffering from orofacial neuropathic pain has increased. These cases usually arise from complications of dental procedures such as root canal treatment (chemical injury), local anesthesia (needle injury), tooth extraction, dental implant surgery, jaw surgery, or trauma [2–5]. Symptoms usually appear in the trigeminal nerve territories including the inferior alveolar nerve (IAN), lingual nerve, and infraorbital nerve [2]. The IAN, which can be affected by various dental procedures, is most vulnerable to injury and can easily be inadvertently damaged during procedures resulting in sensory disturbance in the lower lip and chin skin areas [2–5]. Chronic neuropathic pain causes deleterious effects on the social, mental, physical and economic health of patients, resulting in serious deterioration in quality of life [2, 3, 6, 7]. If neuropathic pain results from iatrogenic damage, increased medical disputes may also occur in consequence [2, 6].

✉ Hyung Jun Kim
kimoms@yuhs.ac

[1] Department of Oral and Maxillofacial Surgery, College of Dentistry, Yonsei University, 50-1, Yonsei-ro, Seodaemun-gu, Seoul 03722, Republic of Korea

[2] Department of Oral and Maxillofacial Surgery, Wonkwang University Sanbon Hospital, 321, Sanbon-ro, Gunpo-si, Gyeonggi-do 15865, Republic of Korea

Accurate assessment of nerve damage is important for diagnosis, treatment, and prognosis of neuropathic pain conditions and can accelerate recovery [3, 6]. Clinical assessment of pain from nerve injury relies heavily on patients' self-reported symptoms, which can be highly subjective. Thus, pain can be very difficult to objectively evaluate [6, 8]. Most nerve injury assessment methods used in clinics for peripheral neurological examination, such as the clinical neurosensory test, Neurometer® Current Perception Threshold (Neurotron, Inc., Baltlmore, Maryland, US), electromyography (EMG), and digital infrared thermal imaging (DITI) are somewhat subjective and invasive, and the anatomical sites of injury are difficult to distinguish. These current methods focus on functional evaluation of the nerve state and provide minimal insight into the dynamics of damage or regenerative mechanisms [3, 4, 6, 9–11]. They can be complemented by histological biopsies, but such tests are restrictive due to their inherent invasiveness. Non-destructive structural and functional assessment of peripheral nerves are necessary to accurately diagnose patients suffering nerve pain [6].

Several publications introduced current and prospective noninvasive imaging techniques for assessment of the nerve state, including computed tomography (CT), magnetic resonance imaging (MRI), diffusion tensor imaging (DTI), ultrasonography (US), positron emission tomography (PET), and other molecular imaging techniques [6, 8, 12]. Among those modalities, PET is suggested as having the most potential for diagnosing peripheral neuropathy [6, 8]. Its advantages include ability to visualize metabolism, high sensitivity and early detection of disease; its disadvantages include local production of rapidly decaying imaging agents and an inability to directly image nerves [6, 8, 13]. In PET, the background tissue activity of radiopharmaceuticals, such as Fluorine-18-fluorodeoxyglucose (^{18}F-FDG), may overwhelm uptake in the region of interest. Thus it is extremely difficult to confidently ascribe any abnormality to an anatomical structure [6, 8]. However, CT and MRI fused with PET can help to clarify the anatomical location abnormalities. Moreover, MRI, which has superior soft tissue contrast, is more suited for examination of peripheral neural tissue [8, 13].

To date, there have been few systematic in vivo studies focusing on the practical efficacy of PET for diagnosing peripheral neuropathy, except in the case of cancerous nerve lesions [9, 13, 14]. The aim of this study was to investigate the efficacy of PET/MRI for diagnosing peripheral nerve injuries using two popular nerve injury models in sciatic nerve of rat: chronic constriction injury (CCI) and crushing injury. One of the most commonly employed animal models of neuropathic pain is CCI [15]. Because the ligation thread used in CCI can induce an inflammatory reaction that may affect PET imaging, a crushing injury model was also used in this study. Paw withdrawal thresholds test and histomorphometric analysis were performed as well. All assessment methods were quantified and evaluated for significance.

Materials and Methods

Animals

Thirteen male Sprague–Dawley rats (7 weeks old; weighing between 200 and 250 g) were used in this study. Rats were housed individually in standard rat cages and maintained under constant temperature and humidity, with a 12-h light/dark schedule. Purified drinking water and a pellet diet were supplied. Animals were allowed to acclimate for 1 week prior to experiments. All animal protocols were approved by the Institutional Animal Use and Care Committee of the Department of Laboratory Animal Resources, Yonsei Biomedical Research Institute, Yonsei University College of Medicine, Korea.

Experimental Design

Two experimental groups (n = 4, respectively), a control group (n = 4) and one normal individual (n = 1) constituted this study (Fig. 1a). Two different models of peripheral nerve injury (CCI, and crushing injury) were used for experimental groups, and sham surgery was performed for the control group. All surgical manipulations were performed in the left sciatic nerves of rats. One rat was preserved intact for procuring natural anatomical images. For the control group, the sciatic nerves were preserved intact. Simply, about 15 mm of the nerve proximal to the sciatic trifurcation was freed with gentle manipulation (Fig. 1d). In the crushing injury group, a curved hemostat was applied on the freed left sciatic nerve proximal to the sciatic trifurcation for 5 min. The length of sciatic nerve injury was about 3 mm, and the locking force between the tips of the forceps was approximately 40 N (Fig. 1e). In the CCI group, four loose ligatures of 4–0 absorbable synthetic braided suture (Vicryl; Polyglactin 910; Ethicon, INC., a Johnson & Johnson company, Somerville, NJ, USA) with spacing of about 1 mm were placed around the freed left sciatic nerve, proximal to the sciatic trifurcation, until a brief twitch was observed (Fig. 1f).

Surgical Procedure

Under respiratory anesthesia using isoflurane (Forane; JW, Korea), the left thigh area was shaved and cleaned with 10% povidone-iodine. A skin incision about 2 cm was made about 0.5 cm posterior from the femur. The fascia of the biceps femoris and the gluteus superficialis were exposed and the sciatic nerve was approached by blunt dissection through the

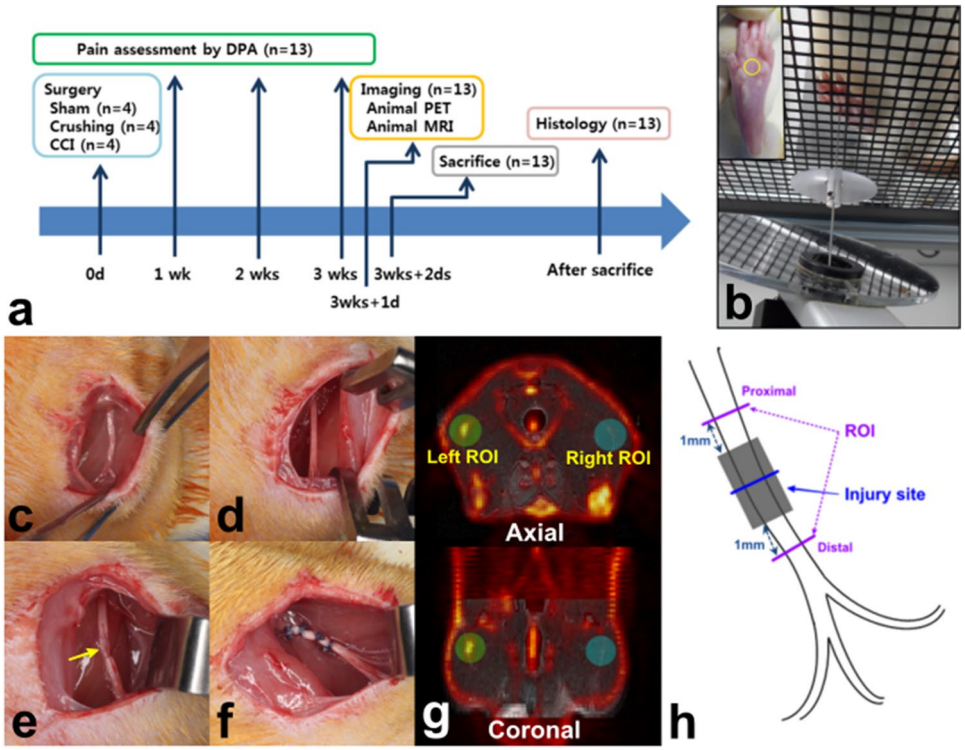

Fig. 1 Experimental design and timeline. **a** Our study involved one rat with no surgery performed and three type of 12 rats with operation on left sciatic nerves; sham (control group), crushing injury and chronic constriction injury (CCI) (experimental groups). Withdrawal thresholds for pain assessment were measured using a Dynamic Plantar Aesthesiometer (DPA) before sciatic nerve injury and at 1, 2, and 3 weeks postoperatively. Animals underwent sequential small-animal PET using the radiotracer, ^{18}F-FDG, and MRI after a half-day fasting. One day after imaging, all animals were sacrificed and the left sciatic nerves were harvested for histologic analysis. **b** Pain behavior assessment by DPA. Rod was pushed continuously and stopped automatically when the rat withdrew his paw (yellow circle area; the test area on the plantar surface of a hind paw). **c** The exposed left sciatic nerve. **d** Sham; about 15 mm of the nerve proximal to the sciatic trifurcation was freed. **e** Crushing injury; a curved hemostat was applied on the freed left sciatic nerve proximal to the sciatic trifurcation for 5 min. **f** CCI; four loose ligatures of 4–0 absorbable synthetic braided suture with spacing of about 1 mm were placed around the freed left sciatic nerve, proximal to the sciatic trifurcation, until a brief twitch was observed. **g** Coregistration of PET and MRI was performed using AMIDE image analysis software. Spherical shaped regions of interest (ROIs), about 6 mm in diameter, were set on the nerve injury site (left) and on the side opposite it. **h** Specimen ROIs. Two cross-sections (4 μm thickness), taken 1 mm proximal and 1 mm distal to the injury site, were mounted on slides, and stained with hematoxylin and eosin (H&E) and toluidine blue (Color figure online)

intermuscular space between them (Fig. 1c). Approximately 15 mm of nerve was carefully freed from the surrounding tissue using micro-pincettes. Nerve damage was formed only in the experimental groups by the two different methods described previously. Surgical sites were closed layer-by-layer with 4-0 Vicryl for muscle and fascia and 5-0 nonabsorbable synthetic monofilament suture (Nylon; AILEE Co., Busan, Korea) for skin. All animals were sacrificed by CO_2 inhalation 3 weeks after surgery. Left sciatic nerves were then harvested for histological analysis.

Pain Behavior Assessment

Before sciatic nerve injury and at 1, 2, and 3 weeks postoperatively, withdrawal thresholds for mechanical stimulation of the rat hind-paw were measured using a Dynamic Plantar Aesthesiometer (DPA; Ugo Basile, Comerio, Italy) [16, 17], which is an automated Von Frey-type system (Fig. 1b). Rats were placed into the DPA test chamber for 15 min to allow acclimation to the environment before the experiment commenced. Through a wire-gated floor, a thin rod with a diameter of 0.5 mm was pushed against the plantar surface of the hind paw. The force was increased from 0 to 50 g over a period of 20 s at a rate of 2.5 g/s. The rod stopped automatically and recorded the latency time after the animal withdrew its paw. The mean of three consecutive trials at intervals of at least 5 min was used for analysis.

Small-Animal PET/MRI

All animals were anesthetized with isoflurane throughout imaging. Animals underwent sequential small-animal PET (Inveon PET; Siemens, Germany) and small-animal MRI (Bruker 9.4 T 20-cm-bore MRI system; Biospec 94/20

USR; Bruker, Ettlingen, Germany). A customized PET table similar to an MRI table was prepared and used to facilitate image superimposition. Approximately 40 MBq of ^{18}F-FDG was injected intravenously, and 1-h dynamic scans of the thigh were obtained, and T2-weighted rapid acquisition with relaxation enhancement (RARE) images of the thighs (repetition time [TR] = 2300 ms; echo time [TE] = 11 ms; slice thickness = 1 mm, acquisition matrix = 192 × 192; acquisition FOV 55 × 55 mm^2) were obtained at 3 weeks postoperatively.

Coregistration of PET and MRI was performed using AMIDE image analysis software (amide.exe 1.0.4; https://amide.sourceforge.net). The MRI images helped to indicate the anatomic location of the sciatic nerves and the placement of the regions of interest (ROIs). Spherical shaped ROIs, about 6 mm in diameter, were set on the nerve injury site and on the side opposite it (Fig. 1g). For quantitative analysis of PET signals, the maximum standardized uptake values (SUV_{max}) of the ROIs were calculated using OsiriX image analysis software (Pixmeo, Geneva, Switzerland). The ratio of the *SUV* (*SUVR*) from two different regions within the same PET image (from a target and a reference region) was also calculated to eliminate differences between the animals as follows:

$$SUVR = SUV_{target} / SUV_{reference} = SUV_{left\ ROI} / SUV_{right\ ROI}$$

Histological and Histomorphometric Analysis

All harvested left sciatic nerves were fixed in 4% paraformaldehyde for 24 h immediately after sacrifice. They were then embedded in paraffin with threads indicating their orientation. For each specimen, two cross-sections (4 µm thickness), taken 1 mm proximal and 1 mm distal to the injury site, were mounted on slides, and stained with hematoxylin and eosin (H&E) and toluidine blue for histological and histomorphometric analysis (Fig. 1h).

For quantitative analysis of histological changes after nerve injury, a fully automated method was used for quantification of myelinated axon numbers on proximal and distal ROIs to the injury site [18]. Toluidine blue slides were whole scanned with × 200 magnification using a digital pathology scanner (Aperio AT2, Leica Biosystems, Wetzlar, Germany), and photomicrographs of the ROIs were acquired using Aperio ImageScope (Leica Biosystems, Wetzlar, Germany) (Fig. 2a). Then the ImageJ software program (Fiji Distribution, National Institute of Health, Bethesda, MA) was used to combine overlapping photomicrographs of each nerve cross section and to create a single stitched composite image representing the entire cross section at × 200 magnification (Fig. 2b). The stitched image was then cropped using a photo editing software program (PhotoScape X, Mooii Tech, South Korea) to remove histological content outside the nerve fascicle, including epineurium, perineurium, and blood vessels within the fascicle (Fig. 2c). The cropped image was converted to the binary image, and the number of myelinated axons was measured in the binary image using ImageJ (Fig. 2d–f) [18].

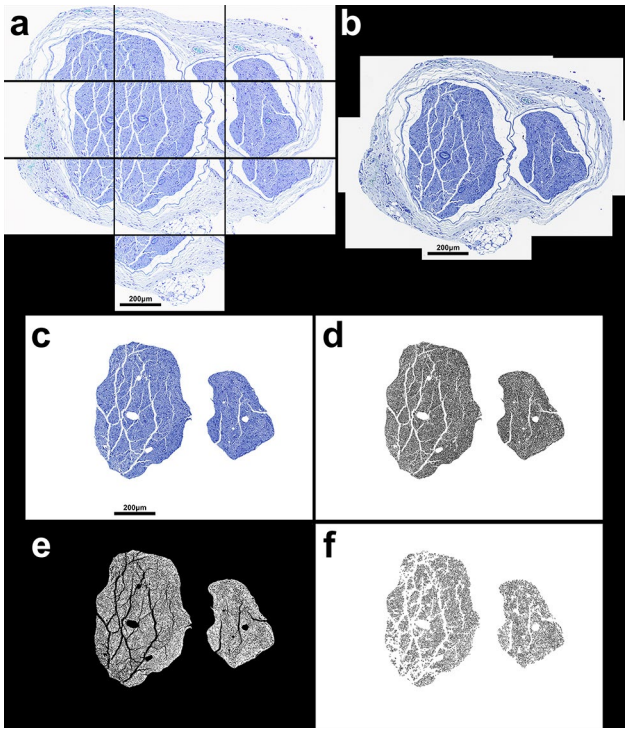

Fig. 2 Image processing for automated counting number of myelinated axons. **a** Photomicrographs of a sciatic nerve section. Ten overlapping photomicrographs of a sciatic nerve cross section were captured at × 200 magnification. The photomicrographs overlap with each other to allow combining into a single photomicrograph using the stitching function in ImageJ. The photomicrographs were stained with toluidine blue and the scale bar represents 200 µm as labeled. **b** The stitched image. The ten photomicrographs from (**a**) are stitched together in ImageJ to give a single × 200 photomicrograph of the normal rat sciatic nerve cross section. **c** The cropped image. The photomicrograph from (**b**) is cropped using PhotoScape X to remove epineurium, perineurium, and large blood vessels. **d** The binary image. The photomicrograph from (**c**) is converted into a binary image using ImageJ. Originally, this allows particle analysis for nerve fiber number in the reference article [18]. However, the thickness of specimen of this study (4 µm) was thicker than that of reference article (0.5 µm), so that some modification was applied as follows. **e** On the inverted black and white image from (**d**), the number of myelinated axons was measured by counting the number of black dots within a certain size range. **f** The image of counted myelinated axons. This figure is a drawing of the myelinated axons that ImageJ outlined and measured for number

Statistical Analysis

Statistics were analyzed using PASW SPSS software (Version 18.0, SPSS Inc., Chicago, IL, USA). First, the Shapiro–Wilk test was used to check normal distribution of the

data. The significance of any differences between two groups was assessed using the non-parametric test for skewed data and the parametric test for normally distributed data; probabilities of 0.05 or less were accepted as significant. Correlation analysis between the three assessment methods was also performed.

Results

Mechanical Threshold Assessment by DPA

Figure 3 shows change with time of the behavial response to non-noxious stimuli on both legs. The paw withdrawal threshold values over time between the control group and the right (uninjured) legs of both experimental groups were similar. However, mechanical allodynia was observed in the left (injured) legs of both experimental groups after nerve injury. The Shapiro–Wilk test demonstrated that most data were normally distributed, except for the left side of the sham surgery group and the right side of the CCI group. The significance of any differences between preoperative and postoperative 3 weeks was assessed using the parametric paired t-test for normally distributed data and the non-parametric Wilcoxon's Signed-rank test was used for skewed data. Probabilities of 0.05 or less were accepted as significant. There were significant differences only in the injured sides of both experimental groups (Crushing injury; $p = 0.002$, and CCI; $p = 0.005$).

Withdrawal threshold values were revised to compensate for different conditions of individual rats (such as sensitivity, nervousness, fear, adaptation and blunting) prior to comparison between variables at postoperative 3 weeks in the three groups. Revised withdrawal threshold values (RevWT) were calculated as follows: *Withdrawal thresholds value of injured side / Average of withdrawal threshold values of intact sides (in each group)*. One-way analysis of variance (ANOVA) demonstrated that the RevWT of the experimental sides were significantly different between the sham surgery and crushing injury groups ($p < 0.0001$), as well as between the sham surgery and CCI groups ($p < 0.0001$). There was no significant difference between the experimental groups ($p = 0.451$). This indicated significant nerve impairment in both experimental groups at 3 weeks after nerve injury (Table 1).

Imaging Analysis

Clear visualization of the anatomical structures was enabled by MRI and the uptake sites were observed in more detail through PET (Fig. 4a). In the control group, there was no significant difference between bilateral ROIs in the

Table 1 Statistical analysis of the assessment methods among the control and experimental groups

	Sham-crushing injury	Sham-CCI	Crushing injury-CCI
RevWT[a]	0.000*	0.000*	0.451
SUVR[a]	0.027*	0.001*	0.067
MAxR[b]	0.051	0.048*	0.149

[a]One-way ANOVA

[b]Games-Howell tests

*$p < 0.05$

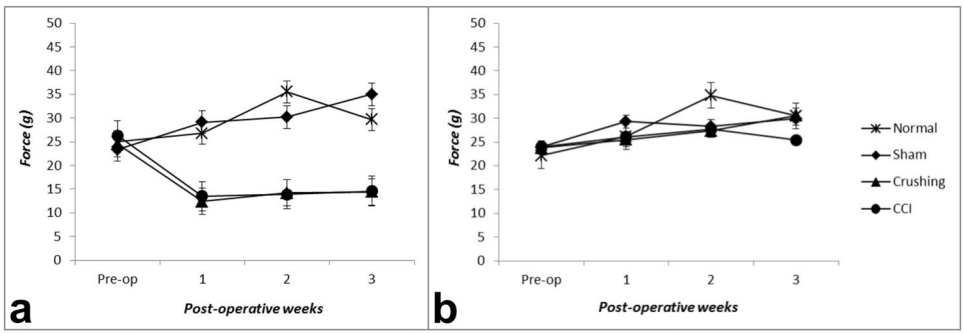

	Sham surgery		Crushing injury		CCI	
	left	*right*	*left*	*right*	*left*	*right*
Pre-op	23.3 (3.8)	23.9 (1.3)	24.5 (3.7)	23.8 (2.5)	26.3 (3.2)	24 (4.4)
POD 3wks	35 (4.9)	29.9 (8.4)	14.4 (2)	30.6 (5)	14.6 (2)	25.4 (3.5)
p value	0.068†	0.253‡	0.002‡*	0.063‡	0.005‡*	0.273†
RevWT	1.17 (0.17)		0.47 (0.07)		0.57 (0.08)	

† Wilcoxon's signed-rank test ‡Paired t test * $p < 0.05$

Revised withdrawal thresholds value = left value/ right mean value

Fig. 3 Time course and statistical analysis of withdrawal threshold values change and revised withdrawal threshold values (RevWT) at postoperative 3 weeks (mean, standard deviation). **a** Injured (left) leg. The mean paw withdrawal threshold significantly decreased at both experimental groups after injury. **b** Intact (right) leg. There is no significant difference of paw withdrawal threshold at all groups. All values on graphs are given as mean ± standard error. $p < 0.05$ for all statistical comparisons

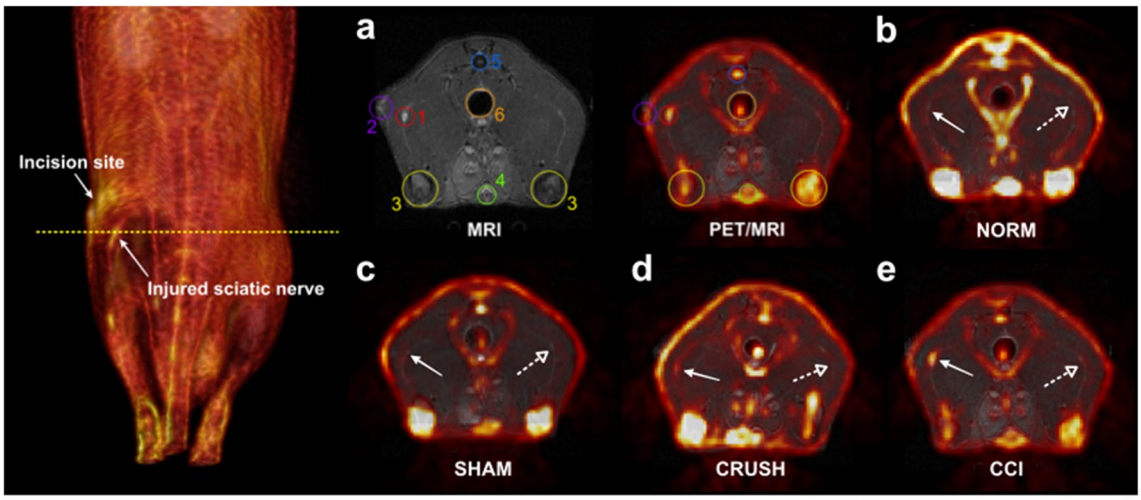

Injury type (left sciatic nerve)			Normal	Sham surgery				Crushing injury				CCI			
Rat (n=13)			1	2	3	4	5	6	7	8	9	10	11	12	13
SUV	SUV_{max} *(g/ml)*	Left	0.794	0.837	0.798	0.879	0.945	1.650	4.808	1.640	1.779	1.907	3.946	3.004	2.869
		Right	0.761	0.829	0.702	0.919	0.753	0.626	1.682	0.770	0.874	0.594	0.820	1.146	0.853
	SUVR (left/right)		1.04	1.01	1.14	0.96	1.25	2.64	2.86	2.13	2.04	3.21	4.81	2.62	3.36
	Mean (Standard deviation)			1.09 (0.13)				2.42 (0.4)				3.5 (0.93)			

Fig. 4 Imaging analysis on PET/MRI. The yellow dotted line indicates the location of PET/MRI slices. **a** Labeled anatomical structures on PET/MRI. 1 = nerve injury site, 2 = incision site, 3 = knee joint, 4 = penile urethra, 5 = vein and tail, 6 = rectum. (b,c,d,e) Representative PET/MRI fused images of all groups. Solid line arrows indicate left ROIs and open-headed dashed arrows indicate right ROIs. There was significant uptake of the nerve injured sites compared to the corresponding uninjured sides only in both experimental groups (crushing injury and CCI). For the quantitative analysis of PET image, SUV_{max} and *SUVR* of ROIs were calculated using OsiriX image analysis software. (NORM; no surgery (normal): rat 1, SHAM; sham surgery group: rat 2–5, CRUSH; crushing injury group: rat 6–9, CCI; CCI group: rat 10–13. The number of the rats does not to correspond to the order of procedures) (Color figure online)

cross-section images as in the non-operated rat (Fig. 4b, c). On the other hand, there was significant uptake of the nerve injured sites compared to the corresponding uninjured sides in both experimental groups (Fig. 4d, e). Calculated SUV_{max} of ROIs and *SUVR* are shown in Fig. 4. Shapiro–Wilk test indicated that all measured *SUV* data were normally distributed. The significance of any differences between the left and right ROIs was assessed using the parametric one sample t-test (test value = 1). Probabilities of 0.05 or less were accepted as significant, and there were significant differences in both experimental groups (Crushing injury; $p = 0.006$, CCI; $p = 0.013$). One-way ANOVA demonstrated that the *SUVR* of both experimental groups was significantly higher than the control group (Crushing injury; $p = 0.027$, CCI; $p = 0.001$). There was no significant difference between the experimental groups ($p = 0.067$) (Table 1).

Histological and Histomorphometric Analysis

Histological Analysis (H&E Staining)

In the sham surgery group, the two ROIs produced similar histologic findings. Dense myelinated axons surrounded with perineurial epithelium were visible in all sections (Fig. 5b,e). The density, and rate of degradation of neural cells did not differ between the experimental and control groups in proximal ROIs (Fig. 5b, h, n). Both samples showed intact and vital cellular features. However, the distal ROIs of the experimental groups showed definite structural disintegration, including fragmentation and atrophy of myelin and axons, swollen neuronal bodies, and interstitial fibrosis within the nerve fibers, compared to the intact control group (Fig. 5k, q). Within the experimental groups, the distal ROI showed an overall atrophic morphology including increased nerve diameter due to pathological swelling. Interestingly, increased numbers of Schwann cells were observed, especially in the distal ROI of crushing injury group (Fig. 5k).

Histomorphometric Analysis (Toluidine Blue Staining)

The number of myelinated axons of the ROIs is shown in Fig. 5. Unlike the sham surgery group, there were significant differences in the myelinated axon counts between the proximal and distal ROIs in both experimental groups (Crushing injury; $p < 0.0001$, CCI; $p = 0.001$). The ratio of the number of myelinated axons at the proximal and distal ROIs (MAxR) was used to analyze intergroup differences.

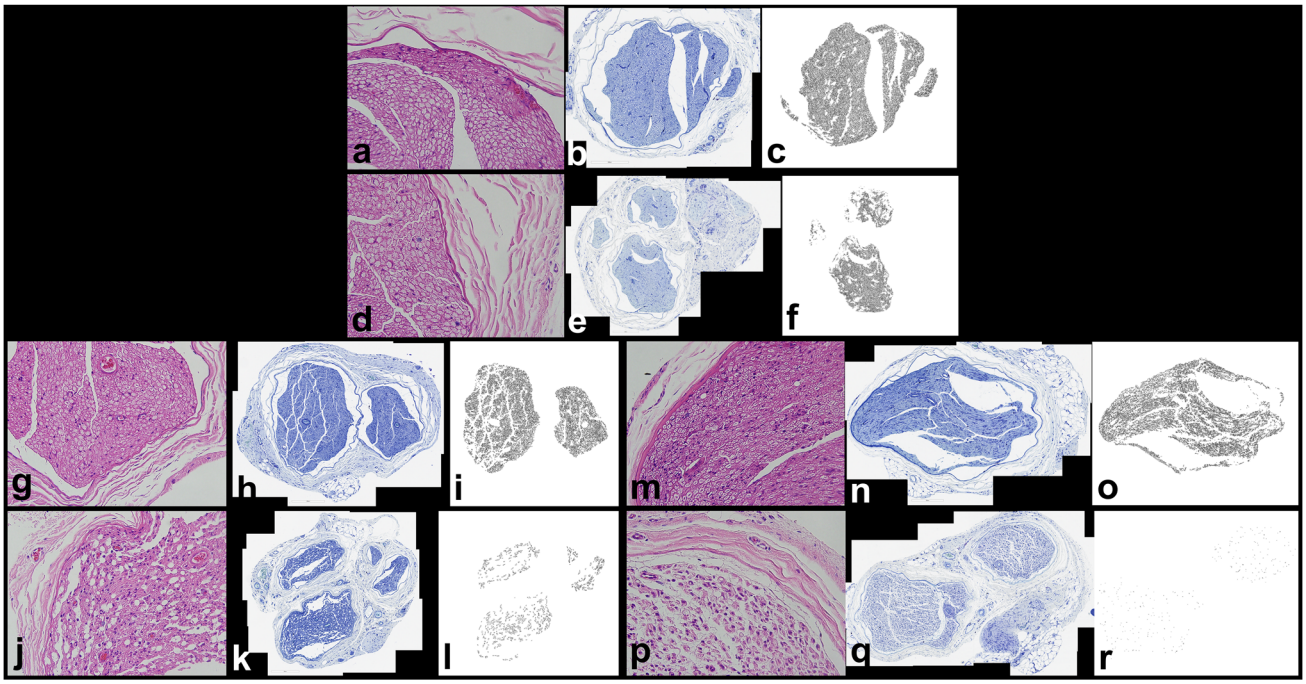

Injury type	Normal	Sham surgery					Crushing injury				CCI		
Rat	1	2	3	4	5	6	7	8	9	10	11	12	13
Proximal	4214	4933	6479	5812	6357	5672	4984	6383	5761	5884	3313	6807	7207
Mean (SD)			5895 (704)				5700 (573)				5803 (1750)		
Distal	3741	5565	5813	4668	5879	685	771	603	1615	446	376	333	280
Mean (SD)			5481 (559)				919 (469)				359 (70)		
MAxR*	1.13	0.89	1.11	1.25	1.08	8.28	6.46	10.59	3.57	13.19	8.81	20.44	25.74
Mean (SD)			1.08 (0.15)				7.23 (2.97)				17.05 (7.52)		

*MAxR (the ratio of the number of myelinated axons at proximal and distal ROIs) = number of axons at proximal ROI/ number of axons at distal ROI

Fig. 5 Histological and histomorphometric analysis. **a**–**c** Proximal ROI of sham group: dense myelinated axons surrounded with perineurial epithelium were visible. **d**–**f** Distal ROI of sham group: same histologic findings as proximal ROI. Mean ± standard deviation(SD) MAxR of sham group was 1.08 ± 0.15. **g**–**i** Proximal ROI of crushing injury group: same histologic findings as proximal ROI of sham group. **j**–**l** Distal ROI of crushing injury group: structural disintegration was observed. The number of myelinated axons was reduced, and mean ± SD MAxR of crushing injury group was 7.23 ± 2.97. **m**–**o** Proximal ROI of CCI group: same histologic findings as proximal ROI of sham group. **p**–**r** Distal ROI of CCI group: more severe degeneration was observed than crushing injury group. Mean ± SD MAxR of CCI group was 17.05 ± 7.52 due to significantly reduced number of myelinated axons of distal ROI. **a**, **d**, **g**, **j**, **m**, **p** × 400 magnification, H&E staining. **b**, **e**, **h**, **k**, **n**, **q** × 200 magnification, stitched images, toluidine blue staining. **c**, **f**, **i**, **l**, **o**, **r** Drawings of the myelinated axons that ImageJ outlined and measured for number. (normal: rat 1, sham surgery: rat 2–5, crushing injury: rat 6–9, CCI: rat 10–13. The number of the rats does not to correspond to the order of procedures)

The homogeneity of variance was low ($p = 0.004$). The Games-Howell test used to analyze the differences of MAxR between the control and experimental groups showed a significant difference between the sham surgery and CCI groups ($p = 0.048$) (Table 1).

Correlation Between Assessment Methods

Pearson correlation analysis was performed to analyze correlations between the three assessment methods (RevWT, *SUVR* and MAxR). There was a high correlation between RevWT and *SUVR* (Pearson's r = − 0.710, $p = 0.010$), and a significant correlation between *SUVR* and MAxR (Pearson's r = 0.611, $p = 0.035$). However, there was no significant correlation between RevWT and MAxR (Pearson's r = − 0.567, $p = 0.055$) (Fig. 6).

Discussion

To date, of the majority of modalities for nerve assessment in patients with peripheral neuropathic pain are relatively subjective and inaccurate. Recent developments in the field of peripheral nerve imaging have presented some possibilities to overcome those obstacles to realize accurate diagnosis for better prognosis of peripheral neuropathy [6, 8, 9, 12]. Several well-known imaging modalities such as CT, MRI, DTI, US and PET, have been proposed for current and prospective imaging of the peripheral nervous system. Current clinical

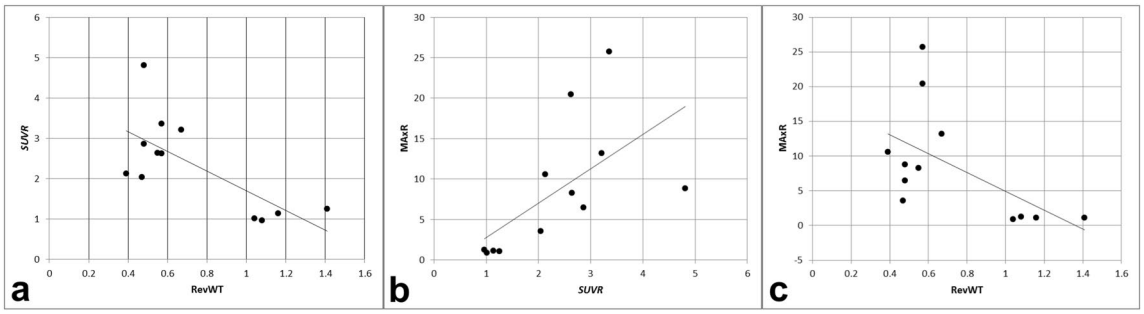

	RevWT-*SUVR*	*SUVR*-MAxR	RevWT-MAxR
Correlation coefficient	-0.710	0.611	-0.567
p value	0.010*	0.035**	0.055

Pearson correlation analysis *$p < 0.01$ **$p < 0.05$

Fig. 6 Correlation analysis between RevWT, *SUVR* and MAxR. **a** Graph of correlation between RevWT and *SUVR*. **b** Graph of correlation between *SUVR* and MAxR. **c** Graph of correlation between RevWT and MAxR. There was a significant correlation between RevWT and *SUVR* (Pearson's r = -0.710, $p = 0.010$), and between *SUVR* and MAxR (Pearson's r = 0.611, $p = 0.035$) except between RevWT and MAxR (Pearson's r = -0.567, $p = 0.055$)

imaging modalities used to evaluate chronic pain include CT, MRI and US. These focus on imaging anatomic alterations only and demonstrate low sensitivity and specificity for the detection of pain-generating pathologies [8, 9]. However, DTI, PET, and other molecular imaging techniques permit the identification of abnormal biological processes (unique physiologic and biomolecular changes causing pain). These modalities show considerable potential because they enable visualization of the degree of nerve injury or metabolism [6–8, 12, 13]. Increased nociceptive activity is associated with increased metabolic, hemodynamic, mediator, and cellular changes. Thus, PET may be applied to each category of molecular mechanism, such as celluar response, inflammatory mediators and receptors, ion channel expression, and metabolic response, to detect abnormal physiologic activity along the nociceptive pathway in the peripheral and central nervous systems [8].

In preclinical stage, metabolic imaging of peripheral neuropathy has been challenged by the relatively poor spatial resolution of small-animal PET for the thin sciatic nerve, approximately 1–2 mm in diameter, in rats [13]. The spatial resolution of small-animal PET varies from 0.7 to 1.84 mm in full width at half maximum in phantom studies (1.4 mm in this study), and small-animal MRI which has high spatial resolution from 0.1 to 0.5 mm (0.28 mm in this study) can solve the difficulty in distinguishing peripheral nerves from background activity using PET alone [6, 8, 13]. The aim of this study was to investigate the capacity of PET to detect damaged peripheral nerves via the metabolic response category of molecular mechanism.

After nerve damage, increased spontaneous activity and metabolic changes contribute to symptoms of neuropathic pain. Neuronal activity is dependent on glucose metabolism [8, 13] and PET imaging can determine regions of high metabolic activity through modified glucose molecules, such as ^{18}F-FDG. FDG is transported across the cell membrane by the same transporters that are responsible for the facilitated transport of glucose. Like glucose, FDG is localized and consumed in proportion to metabolic demand. The ^{18}F releases a positron that rapidly annihilates with an electron, producing γ photons whose positions are determined by the PET imager and used to produce a map of the ^{18}F-FDG [6, 8, 19]. Owing to this mechanism, PET imaging has very high sensitivity and can be used for the early detection of disease [6, 8]. Despite its promising potential in this field, there have been few systematic studies of PET imaging in the peripheral nerves in noncancerous settings.[6, 9, 13, 14]

Meanwhile, the potential effects of inflammatory response from nerve injury on FDG uptake should be also considered for reading PET imaging in peripheral neuropathy. Local nerve injury can influence the lumped constant (LC), a correction factor used to infer glucose metabolic rate from FDG metabolic rate, and it might be critical in quantitative calculation of regional glucose metabolic rates when FDG is used as the tracer [19, 20]. In the cytoplasm, FDG is phosphorylated by hexokinase, and at that point its metabolism ceases except for very slow dephosphorylation, therefore the accumulation rate of FDG is proportional to the metabolic rate. However, transport and phosphorylation of the 2 hexoses occur at somewhat different rates so a correction factor, LC, is necessary to convert FDG metabolic rate to the glucose metabolic rate [19]. It is possible that the inflammatory response reduces the glucose concentration in the damaged nerve, thereby increasing the phosphorylation

of FDG and increasing the relative *SUV*. This can make PET imaging increase the ability to detect the site of nerve damage with higher metabolic rate. On the other hand, it is also possible that when blood-nerve barrier collapses due to inflammation, increasing local glucose concentration, the phosphorylation of FDG may be depressed reducing the relative *SUV*. This possibilities may interrupt understanding the exact current status of injured nerve through PET imaging therefore further research on this issue will be necessary, such as determining independently metabolic rates of both FDG and glucose using PET imaging for measuring the LC or comparing of periodic serial PET scans quantitatively during subsiding inflammation after nerve injury [19].

Various animal models of nerve injury have been developed for studying the mechanisms of neuropathic pain and the development of effective therapy for its optimal management [15]. One of the most commonly used animal models of neuropathic pain is the CCI model of peripheral mononeuropathy developed by Bennett and Xie [14, 15, 21]. In this model, constriction of the sciatic nerve induces intraneural edema, focal ischemia, and Wallerian degeneration [15]. Previously documented behavioral signs of spontaneous pain include autotomy, guarding, excessive licking, limping of the ipsilateral hind paw, and avoidance of placing weight on the injured side [15, 22]. In this study, contracture formation of the affected paw was also observed. Changes of sensation, such as mechanical and thermal hyperalgesia, chemical hyper-reactivity, and cold allodynia have been reported to develop within a week, and they can persist for over seven weeks after CCI surgery [15]. Partial damage to the nerve leads to sensitization of both A- and C-fibers, and plays a role in initiating and maintaining pain behaviors [15]. However, there has been a degree of variation observed between the CCI models, which may be explained by varying tightness of the constriction produced by tying knots with sutures, the types of suture material, and the different strains of rat [15]. For this reason, this study used revised values (RevWT) for comparison of intergroup withdrawal threshold values. In this study, the author used 4-0 Vicryl instead of 4-0 chromic gut, which was used for the original CCI model. This is because PET may be affected by tissue reaction to suture materials and Vicryl shows less inflammatory reaction than a chromic gut [23]. The potential for localized inflammatory response to surgical sutures affecting PET imaging was one reason that the additional injury model which did not require foreign materials such as thread was used in this study.

The crushing injury model is also widely used for research into peripheral nerve injury [17, 24–26]. Pilot studies in which 60 g force vascular clips (Micro Serrefines; Fine Science Tools, North Vancouver, British Columbia, Canada) or hemostatic forceps were applied for 2 or 5 min influenced the decision to use curved hemostat forceps for 5 min in the current study. This decision was based on the rational that this was the first PET imaging study to use a crushing nerve injury model and the injury needed to be sufficient to be clearly detected by PET. In the current study, pain behavior assessment indicated that RevWT was not significantly different between CCI and crushing injury groups. However definite improvement in the degree of contracture of the affected paws, as well as better walking were observed in the crushing injury group in contrast to the CCI group, although no other behavior assessments (such as walking track analysis) were performed [22]. The recovery of nerve function in the crushing injury group was quicker than that of the CCI group, probably because the degree of nerve injury caused by crushing injury was relatively weak compared to CCI.

In the current study, withdrawal threshold tests using DPA and counting the number of myelinated axons were performed to assess peripheral nerve damage and used to verify the diagnostic efficacy of PET/MRI as a new imaging modality in peripheral nerve injury. The withdrawal threshold test was used as a clinical neurosensory test, and it was somewhat subjective and changeable depending on the conditions of the animals and the environment during testing. DPA, the automated filaments for evaluation of neuropathic pain, was a convenient and useful piece of equipment used in place of the commonly used Von Frey filaments [17, 27] However, there was difficulty using the DPA in the CCI model owing to the paw deformity and change in foot posture [27]. To overcome these limitations, it was necessary to perform the assessment on a stable animal at a fixed time of the day with sufficient time for adaptation. Also, it was sometimes necessary to wait a period of time to reliably test the rat. On the other hand, histomorphometric analysis is regarded as an objective assessment of injured nerve [6]. After peripheral nerve injury, several histological changes occur distal to the injury site as follows: increased inflammatory reactions, edema in epineurium, fibrosis in the nerve fibers, axonolysis, decreased number of regenerating myelinated axons, and reduced diameter of myelinated axons [24, 26, 28]. These changes can also be detected proximal to the injury site due to a combination of retrograde Wallerian degeneration and the development of certain axonal sprouts that become directed centrally due to obstruction at the repair site [28]. In this study, the proximal ROI of each specimen was set 1 mm from the proximal margin of the injury site. Significant degenerative changes were not observed at the proximal ROI. To quantify the histologic findings, the author counted the number of myelinated axons at the proximal and distal ROI using computerized morphometric analysis [18]. Because the thickness of the tissue specimens in this study were eight times thicker (4 μm) than one reference article (0.5 μm) [18], the author applied a few simple modifications to the original process. All slides were analyzed under the same conditions as each other, and

statistical analysis showed that there was no difference in the number of myelinated axons in the uninjured proximal ROIs between all groups (one-way ANOVA, Sham surgery-Crushing injury; $p = 0.968$, Sham surgery-CCI; $p = 0.993$, and Crushing injury-CCI; $p = 0.991$), therefore the result appeared to be reliable.

Although this was a preliminary study with a small sample size, it demonstrated the usefulness and potentiality of PET imaging for the diagnosis of peripheral nerve injuries. There was no statistically significant difference in the intergroup comparison of *SUVR* between the crushing injury and the CCI groups ($p = 0.067$), but this may have been caused by the small sample size. Only a few lesions of some rats of the experimental groups were visible on the MRIs which were taken to clarify anatomic landmarks. However, the *SUV* values of PET scans were clearly different between the injured and intact side, even for ROIs that were seemingly normal on MRI. These results demonstrate the plausibility of PET for quantifying the extent of nerve damage and its excellent ability to detect even minor nerve damage. Furthermore, results of the correlation analysis indicated that *SUVR* had high correlation with RevWT and MAxR and there was no significant correlation between RevWT and MAxR. Considering that current clinical approaches for nerve-damage evaluation can be quite subjective, PET has considerable potential as a valuable diagnostic tool for peripheral nerve injury.

Additionally, significantly higher signal intensity on MRI and increased uptake of ^{18}F-FDG on PET scan were observed in the nerve-injured side of gastrocnemius calf-muscles of the experimental groups. This implies that persistent denervation may induce metabolic changes within the muscle which may progress to muscle fiber atrophy. Increased fat content and denervated muscle result in glucose hypermetabolism and thus ^{18}F-FDG PET/MRI imaging may be used as a noninvasive modality for the evaluation of peripheral neuromuscular disorders [10, 12, 13, 29].

Recently, several publications explored diagnostic modalities for neuropathic pain and nerve injury using animal models [7, 9, 14]. In future, diagnostic imaging for neuropathic pain and nerve injury will probably use molecular biomarkers or unique contrast agents applied to specific mechanism in nerve injury or neuroinflammation process [6-9, 12, 25]. For example, increased uptake of tracer ^{18}F-FTC-146, which is a highly specific radiolabeled sigma-1 receptor ligand, correlated with Schwann cells and macrophage proliferation during the nerve damage process [8, 9]. Although research indicates the development of more accurate and objective tools for the diagnosis of pain, implementation remains challenging [8]. Obstacles include accounting for the subjective and affective components of pain, determining the accuracy of preclinical animal pain models when applied to the complex human pain experience, and imaging small structures of interest such as peripheral nerves [8]. Development of molecular biomarkers or contrast agents to extend the capability of current imaging modalities such as PET and MRI, combined with other multimodal assessments of neuropathic pain will allow doctors to accurately diagnose and tailor specific treatment options for pain caused by nerve damage [6-9, 14].

Peripheral neuropathy diagnosis remains challenging because conventional assessment modalities do not always correspond to clinical presentation. Through this study, the author was able to demonstrate that the PET scan may be a valuable imaging modality to enable noninvasive, objective diagnosis of neuropathic pain caused by peripheral nerve injury. Also, MRI fused with PET may help clarify the anatomic location of soft tissue structures, including the peripheral nerves.

Acknowledgements The author thanks professor Jae Young Kim, in the Department of Oral and Maxillofacial Surgery at Gangnam Severance Dental Hospital, Yonsei University College of Dentistry, and Dr. Hye Yeong Lee, in the Department of Neurosurgery, Spine & Spinal Cord Institute, Yonsei University College of Medicine, for devoted supporting this study. This study was supported by the Yonsei University College of Dentistry (6-2-16-0019).

Funding This study was funded by the Yonsei University College of Dentistry (6-2-16-0019).

Compliance with Ethical Standards

Conflict of interest The authors declare that they have no conflict of interest.

Ethical Approval All procedures performed in studies involving animals were in accordance with the ethical standards of the Institutional Animal Use and Care Committee of the Department of Laboratory Animal Resources, Yonsei Biomedical Research Institute, Yonsei University College of Medicine, Korea.

References

1. Meacham K, Shepherd A, Mohapatra DP, Haroutounian S (2017) Neuropathic pain: central vs. peripheral mechanisms. Curr Pain Headache Rep 21(6):28. https://doi.org/10.1007/s11916-017-0629-5
2. Ahn DK, Park MK (2011) Animal models for orofacial neuropathic pain. Hanyang Med Rev 31(2):107–115
3. Kim YW, Kim MR (2002) Diagnostic efficacy of DITI (digital infrared thermographic imaging) for the dysesthesia of the lower lip & chin. J Korean Assoc Oral Maxillofac Surg 28:53–60
4. Park JH, Ryu JW, Ahn JM, Ok SM, Yoon CL (2010) Analysis of current perception threshold (CPT) change after dental surgery using neurometer. J Oral Med Pain 35(4):293–298
5. Park JH, Lee SH, Kim ST (2010) Pharmacologic management of trigeminal nerve injury pain after dental implant surgery. Int J Prosthodont 23(4):342–346
6. Rangavajla G, Mokarram N, Masoodzadehgan N, Pai SB, Bellamkonda RV (2014) Noninvasive imaging of peripheral nerves.

Cells Tissues Organs 200(1):69–77. https://doi.org/10.1159/000369451
7. Vasudeva K, Andersen K, Zeyzus-Johns B, Hitchens TK, Patel SK, Balducci A, Janjic JM, Pollock JA (2014) Imaging neuroinflammation in vivo in a neuropathic pain rat model with near-infrared fluorescence and (1)(9)F magnetic resonance. PLoS ONE 9(2):e90589. https://doi.org/10.1371/journal.pone.0090589
8. Tung KW, Behera D, Biswal S (2015) Neuropathic pain mechanisms and imaging. Semin Musculoskelet Radiol 19(2):103–111. https://doi.org/10.1055/s-0035-1547371
9. Shen B, Behera D, James ML et al (2017) Visualizing nerve injury in a neuropathic pain model with [(18)F]FTC-146 PET/MRI. Theranostics 7(11):2794–2805. https://doi.org/10.7150/thno.19378
10. Yamabe E, Nakamura T, Oshio K, Kikuchi Y, Ilegami H, Toyama Y (2008) Peripheral nerve injury: diagnosis with MR imaging of denervated skeletal muscle-experimental study in rats. Radiology 247(2):409–417
11. Audit and Evaluation Advisory Committee (1999) Technology review: the neurometer current perception threshold (CPT). Muscle Nerve 22:523–531
12. Ohana M, Moser T, Moussaoui A, Kremer S, Carlier RY, Liverneaux P, Dietemann JL (2014) Current and future imaging of the peripheral nervous system. Diagn Interv Imaging 95(1):17–26. https://doi.org/10.1016/j.diii.2013.05.008
13. Behera D, Jacobs KE, Behera S, Rosenberg J, Biswal S (2011) ^{18}F-FDG PET/MRI Can be used to identify injured peripheral nerves in a model of neuropathic pain. J Nucl Med 52:1308–1312
14. Lasko L, Huang X, Voorbach MJ, Lewis LG, Stavropoulos J, Carriker J, Seifert TR, Baker SJ, Upadhyay J (2013) Multimodal assessment of nervous and immune system responses following sciatic nerve injury. Pain 154(12):2782–2793. https://doi.org/10.1016/j.pain.2013.08.016
15. Jaggi AS, Jain V, Singh N (2011) Animal models of neuropathic pain. Fundam Clin Pharmacol 25(1):1–28. https://doi.org/10.1111/j.1472-8206.2009.00801.x
16. Yagasaki Y, Hayashi M, Tamura N, Kawakami Y (2013) Gamma knife irradiation of injured sciatic nerve induces histological and behavioral improvement in the rat neuropathic pain model. PLoS ONE 8(4):e61010. https://doi.org/10.1371/journal.pone.0061010
17. Lee HY, Lee HL, Yun Y, Kim JS, Ha Y, Yoon DH, Lee SH, Shin DA (2015) Human adipose stem cells improve mechanical allodynia and enhance functional recovery in a rat model of neuropathic pain. Tissue Eng Part A 21(13–14):2044–2052. https://doi.org/10.1089/ten.TEA.2014.0713
18. Tobin CA, Wang Z, Zhang LL, Agresti M, Grewal P, Matloub HS, Yan JG (2014) A new computerized morphometric analysis for peripheral nerve study. J Reconstr Microsurg 30(2):75–82. https://doi.org/10.1055/s-0033-1354738
19. Graham MM, Muzi M, Spence AM, O'Sullivan F, Lewellen TK, Link JM, Krohn KA (2002) The FDG lumped constant in normal human brain. J Nucl Med 43(9):1157–1166
20. Richner M, Ferreira N, Dudele A, Jensen TS, Vaegter CB, Goncalves NP (2018) Functional and structural changes of the blood-nerve-barrier in diabetic neuropathy. Front Neurosci 12:1038. https://doi.org/10.3389/fnins.2018.01038
21. Xie GJBaY-K, (1988) A peripheral mononeuropathy in rat that produces disorders of pain sensation like those seen in man. Pain 33:87–107
22. Sarikcioglu L, Demirel BM, Utuk A (2009) Walking track analysis: an assessment method for functional recovery after sciatic nerve injury in the rat. Folia Morphol 68(1):1–7
23. Yaltirik M, Dedeoglu K, Bilgic B, Koray M, Ersev H, Issever H, Dulger O, Soley S (2003) Comparison of four different suture materials in soft tissues of rats. Oral Dis 9:284–286
24. Somay H, Emon ST, Uslu S, Orakdogen M, Meric ZC, Ince U, Hakan T (2017) The histological effects of ozone therapy on sciatic nerve crush injury in rats. World Neurosurg 105:702–708. https://doi.org/10.1016/j.wneu.2017.05.161
25. Hill BJ, Padgett KR, Kalra V, Marcillo A, Bowen B, Pattany P, Dietrich D, Quencer R (2018) Gadolinium DTPA enhancement characteristics of the rat sciatic nerve after crush injury at 4.7T. AJNR Am J Neuroradiol 39(1):177–183. https://doi.org/10.3174/ajnr.A5437
26. Turedi S, Yulug E, Alver A, Bodur A, Ince I (2018) A morphological and biochemical evaluation of the effects of quercetin on experimental sciatic nerve damage in rats. Exp Ther Med 15(4):3215–3224. https://doi.org/10.3892/etm.2018.5824
27. Nirogi R, Goura V, Shanmuganathan D, Jayarajan P, Abraham R (2012) Comparison of manual and automated filaments for evaluation of neuropathic pain behavior in rats. J Pharmacol Toxicol Methods 66(1):8–13. https://doi.org/10.1016/j.vascn.2012.04.006
28. Ngeow WC, Atkins S, Morgan CR, Metcalfe AD, Boissonade FM, Loescher AR, Robinson PP (2011) Histomorphometric changes in repaired mouse sciatic nerves are unaffected by the application of a scar-reducing agent. J Anat 219(5):638–645. https://doi.org/10.1111/j.1469-7580.2011.01419.x
29. Lee SH, Oh BM, Lee G, Choi H, Cheon GJ, Lee SU (2014) Feasibility of 18F-FDG PET as a noninvasive diagnostic tool of muscle denervation: a preliminary study. J Nucl Med 55(10):1737–1740. https://doi.org/10.2967/jnumed.114.140731